Permeability and formation factor in compressed expanded graphite

2001 J. Phys.: Condens. Matter 13 4387

(http://iopscience.iop.org/0953-8984/13/20/302)

INSTITUTE OF PHYSICS PUBLISHING JOURNAL OF PHYSICS: CONDENSED MATTER

J. Phys.: Condens. Matter **13** (2001) 4387–4403 www.iop.org/Journals/cm PII: S0953-8984(01)22655-1

Permeability and formation factor in compressed expanded graphite

A Celzard[1] **and J F Marêché**

Laboratoire de Chimie du Solide Minéral, Université Henri Poincaré, Nancy I, UMR—CNRS 7555, BP 239, 54506 Vandoeuvre-lès-Nancy, France

E-mail: alain.celzard@lcsm.uhp-nancy.fr

Received 8 March 2001

Abstract

The permeabilities and the formation factors of an anisotropic block of compressed expanded graphite are measured in gas permeation and ion diffusion experiments, respectively. The critical pore diameter of the material is obtained from mercury-injection experiments carried out on the material, according to the work of Katz and Thompson (Katz A J and Thompson A H 1986 *Phys. Rev.* B **34** 8179, 1987 *J. Geophys. Res.* **92** 599). Other length scales related to transport are obtained from the theory of Johnson *et al* (Johnson D L, Koplik J and Schwartz L M 1986 *Phys. Rev. Lett.* **57** 2564) and are calculated on the basis of several models of pore structure available from the literature. All of these different data are compared, and only the model for which the pores are cylinders of lengths l and diameters δ such that $l = \delta$ is shown to work. This finding is confirmed by the formation factor derived from the experimental values of the permeabilities and the kind of pore structure considered: again, only that for which $l = \delta$ leads to consistent results. Finally, the latter model and the theory of Katz and Thompson are used to estimate both the permeability and the formation factor of the blocks of compressed expanded graphite. A very good agreement is found between the estimate and the experimental results.

1. Introduction

Among the properties of porous media, the porosity Φ, which is the ratio of pore volume to total volume of the sample, is the most important. However, Φ is just a single number and hence cannot suffice to characterize the complex pore-space geometry. Other properties are thus necessary. The permeability k is probably the second most important property of a porous system, and much experimental and theoretical work has been devoted to this physical quantity in the last three decades [1–3]. Indeed, k is a very complex function of the pore space; it both

[1] Author to whom any correspondence should be addressed. Postal address: Laboratoire de Chimie du Solide Minéral, UMR 7555, Université Henri Poincaré, Nancy I, BP 239, 54506 Vandoeuvre-lès-Nancy, France. Telephone: 33(0) 383 912187; fax: 33(0) 383 912568.

0953-8984/01/204387+17$30.00

depends on the absolute sizes of the voids and is very sensitive to the topology of the connected part of the pore network. Another interesting property is the so-called formation factor F; the name originates from geology: study of the electrical properties of rock formations. F is an adimensional parameter defined for materials whose pore space is saturated with a conducting fluid, like brine. It is simply the ratio of the conductivity of the free electrolyte (σ_0) to that of the saturated porous material (σ), provided that the solid phase is insulating. By virtue of Einstein's equation, F is also the ratio of the corresponding diffusivities of the ions responsible for the conductivity of the saturating fluid. It depends only on the geometry of the pore space. Finally, the tortuosity factor τ may be defined in terms of the formation factor and the porosity as $\tau = F\Phi$. Unlike the permeability k, the parameters F and τ are scale-invariant quantities, meaning that if the sizes of the pores and that of the solid grains are magnified or shrunk, leaving the porosity unchanged, their values are unaffected. Since one of the three properties Φ, k or F is often more easily measured than the others, depending on the materials, much effort was made to find cross-property relations between them [4, 5]. For example, the well-known Kozeny–Carman theory has been used many times to describe the permeability behaviour of simple porous systems [1, 2, 6, 7].

In the present study, attempts are made to calculate some of these properties from the measurements of others for a highly porous material such as compressed expanded graphite. This material and the method used for measuring the permeability and the formation factor are described in section 2. The theories which are used to study the properties of porous media, namely that of Kozeny and Carman (KC), that of Johnson, Koplik and Schwartz (JKS) and that of Katz and Thompson (KT) are briefly developed in section 3. According to KT, the permeability and the formation factors are calculable from the knowledge of a critical pore diameter derived from mercury-injection experiments. However, the corresponding equations and more exactly the constant prefactors—see section 4—have been criticized many times and hence should not be applied directly. Indeed, it has been shown that these prefactors depend on the pore structure. Prior to making any calculation, a suitable model of the pore space should be identified. This is achieved in section 5 by comparison of experimental values of the permeability and formation factor with KC, JKS and KT theoretical results, which are all very similar for a given model of pore structure. Next, suitable prefactors for KT equations are obtained, and calculation of k and F is performed in section 6 according to the KT theory.

2. Material and measurements

2.1. Compressed expanded graphite

Expanded graphite (EG) is obtained by subjecting natural graphite flakes inserted by sulphuric acid to a brutal thermal shock. The sudden volatilization of the intercalate induces a huge unidirectional expansion of the initial platelets: highly porous worm-like 'accordions' of graphite are obtained [8–12]. This very light material is characterized by an apparent density of 7.5 kg m^{-3} and a surface area close to 40 m^2 g^{-1}, and its individual particles possess an intrinsic mean porosity of about 99.3% [13]. The description, properties and applications of EG are abundantly detailed in the literature [10, 14–18] and hence are not discussed here. Highly porous cubes may be obtained by uniaxial compaction of expanded graphite in a parallelepiped tube [13, 19]. Some of the potential uses of such consolidated materials, namely as chemical heat pumps [20–23] or supports for active carbons or catalysts [19, 24], require a good permeability of the graphite matrix. Indeed, this property is of first importance since it governs the access of a given fluid to the active sites dispersed on the graphite surface. In this paper, a cube of side 2 cm made of expanded graphite compressed at a density of 140 kg m^{-3}

is investigated in terms of permeability and formation factor. The choice of that particular density originates from the fact that a good compromise is found between permeability and electrical and thermal conductivities, these properties varying in opposite ways as the density of the compressed EG increases [25].

Owing to the obvious orientation of the graphite flakes induced by the uniaxial compression, anisotropic materials are obtained [13, 26]. Thus, compressed EG is a transverse isotropic material [26, 27]. Consequently, the two directions of measurement $\vec{a}$ and $\vec{c}$ shown in figure 1 are defined, and the permeability tensor may be written as follows:

$$\vec{\vec{k}} = \begin{pmatrix} k_a & 0 & 0 \\ 0 & k_a & 0 \\ 0 & 0 & k_c \end{pmatrix}. \tag{1}$$

k_a is the permeability measured parallel to the bedding plane of the graphite flakes (xy-plane), i.e., perpendicular to the pressing stress, while k_c corresponds to the orthogonal direction (z-axis). As dictated by the experimental set-up described below, two different samples are needed to get k_a and k_c.

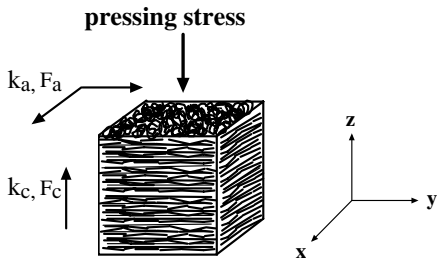

Figure 1. Definition of two orthogonal directions of measurement for both the permeability k and the formation factor F. $\vec{a}$ is the direction parallel to the bedding plane of the graphite flakes (xy-plane), i.e., normal to the pressing stress, whereas $\vec{c}$ is the one perpendicular to the bedding plane (z-axis), i.e., parallel to the pressing stress.

2.2. Permeability measurements

The permeability k is measured as indicated in figure 2, by causing a gas to flow throughout the compressed expanded graphite. For that purpose, the cubic sample is introduced in a tube, which is next filled with a viscous glue. The latter neither affects the porosity of the material nor covers any part of the opposite faces of the sample through which the gas must flow. The tube is then placed into a close-fitting vessel, and nitrogen is forced to flow through the sample with various inlet pressures P_1. During each experiment, P_1 is kept constant, while both the flow rate Q and the pressure drop $\Delta P = P_1 - P_2$ (P_2 being the outlet pressure), are simultaneously measured.

The calculation of the permeability is based on application of Darcy's law [1, 2], which is the hydraulic analogue of Ohm's law for electrical conductivity, of Fick's law for diffusion and of Fourier's law for heat flow. The 'absolute permeability' κ is the constant of proportionality between the velocity $\vec{v}$ of the fluid and the pressure gradient $\vec{\nabla} P$ over the sample:

$$\vec{v} = -\kappa \, \vec{\nabla} P. \tag{2}$$

According to this definition, the permeability is a function of both the pore phase and the nature of the fluid. Hence, an 'intrinsic permeability' k is defined which takes into account the

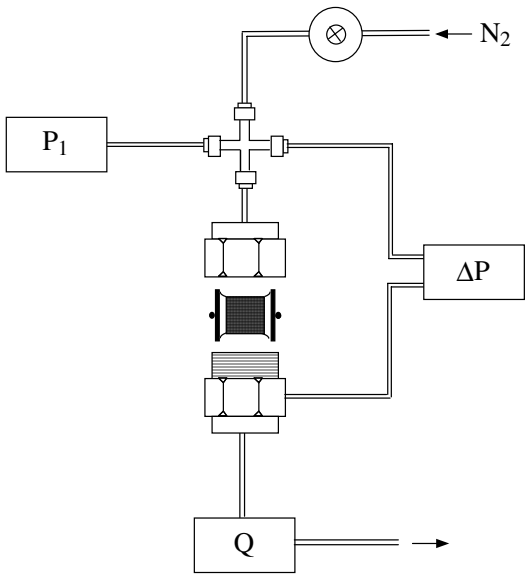

Figure 2. A schematic view of the device with which the permeability is measured. The cubic sample is inserted into a close-fitting vessel (here shown open), and nitrogen is forced to flow throughout it. The inlet pressure P_1, pressure drop ΔP and flow rate Q are measured simultaneously.

dynamic viscosity η of the fluid:

$$k = \kappa\eta. \tag{3}$$

Then, k depends only on the porous medium and has the dimension of area. For an incompressible fluid, one gets

$$k = Q\frac{L}{S}\left(\frac{\eta}{P_1 - P_2}\right) \tag{4}$$

where L is the thickness of the sample and S its cross-sectional area. A very common unit for k is not the square metre but the Darcy (D), which is defined as follows: $k = 1$ D if $\Delta P = 1$ atm, $Q = 1$ cm^{-3} s^{-1}, $S = 1$ cm^2, $L = 1$ cm and the viscosity of the fluid $\eta = 1$ cP, thus corresponding to water. Hence, 1 mD $\approx 10^{-15}$ m^2.

For a compressible fluid like a gas, the velocity is calculated by integrating the differential form of Darcy's law using the condition that is appropriate to gas flow: at constant temperature and steady state, the pressure $\times$ velocity product is constant throughout the sample [2]. Thus, one gets

$$v = -\frac{k}{\eta}\left(\frac{P_2^2 - P_1^2}{2P_2L}\right) \tag{5}$$

and hence

$$k = -Q\frac{L}{S}\eta\left[\frac{2(P_1 - \Delta P)}{(P_1 - \Delta P)^2 - P_1^2}\right]. \tag{6}$$

In figure 3(a), the permeability calculated with equation (6) is plotted as a function of the inlet pressure P_1. It is seen that k depends on P_1; this situation is rather common for gases

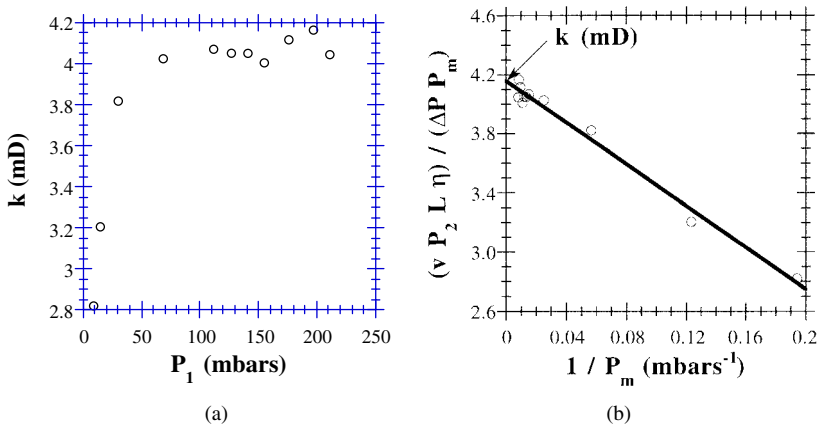

Figure 3. (a) Permeability (measured in the direction $\vec{a}$ and calculated according to equation (6)) plotted as a function of the inlet pressure P_1. (b) Application of Klinkenberg's equation (7) in order to extract the permeability extrapolated to infinite pressure (intercept).

[2, 3]. Consequently, Klinkenberg's equation [2], which allows one to extrapolate k in the limit of an infinite pressure, is applied. It reads

$$\frac{v P_2 L \eta}{\Delta P \, P_m} = k \left[1 + \frac{b}{P_m} \right] \tag{7}$$

where P_m is the average pressure such that $P_m = (P_1 + P_2)/2 = (2P_1 - \Delta P)/2$, and b is the so-called Klinkenberg constant, depending on both the gas and the pore phase. The application of equation (7) is presented in figure 3(b): the permeability is the intercept of the straight line. Thus, the value $k_a \approx 4.16$ mD is found. Similar measurements along the z-axis (see figure 1) and subsequent treatments of the data lead to $k_c \approx 2.25$ mD.

2.3. Formation factor measurements

As stated above, the formation factor F is defined as the ratio σ_0/σ, σ_0 being the conductivity of a given electrolyte and σ that of the pore space of the material studied, saturated with the same electrolyte. Thus, F characterizes the effective resistance to current flow throughout the sample. Nevertheless, since graphite is highly conducting, F cannot be obtained from usual resistivity measurements of the impregnated material. This is why the derivation of the formation factor requires the measurement of the diffusivities of the ions both within the electrolyte alone (D_0) and throughout the saturated pore volume (D). Then, $F = D_0/D$.

The diffusion cell used for measuring the formation factors in the two directions $\vec{a}$ and $\vec{c}$ defined previously is presented in figure 4. It is immersed in a thermostatic bath kept at 25 °C. The cubic sample of compressed expanded graphite is first included and glued into a Teflon block which fits perfectly the inner walls of the beaker subsequently used for the diffusion experiment. The resultant block is then immersed into water laced with wetting agents, and the porous sample is subjected to several successive vacuum–pressure cycles. The impregnation of the material is assumed to be complete after three such cycles. At the beginning of the diffusion experiment, the bottom compartment (referred to as compartment No 1) contains a molar aqueous solution of copper sulphate, while the solution above the saturated sample (referred to as compartment No 2) is free of ions. Compartment No 2 is gently stirred by having small bubbles blown into the solution by a small air pump. The conductivity of the

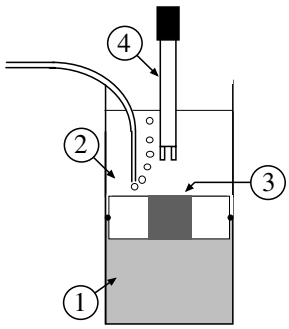

Figure 4. A schematic view of the device with which the formation factors are measured. The cubic sample is inserted into a Teflon block separating two compartments. 1: compartment No 1 containing a molar aqueous solution of $CuSO_4$; 2: compartment No 2; 3: the sample of compressed expanded graphite; 4: the electrode cell for the measurement of the ionic conductivity. Compartment No 2 is gently stirred by having small bubbles blown into the solution by a small air pump.

top compartment is measured as a function of time, using a Consort K912 conductimeter. The latter is equipped with a four-pole Sentek electrode cell having a built-in Pt1000 temperature compensator and a resolution of 0.01 μS cm^{-1}.

Prior to the determination of the diffusion coefficients throughout the material, the increase of the concentration of the ions in compartment No 2 must be calculated via a calibration curve. The latter, obtained by measuring the conductivities at 25 °C of a number of solutions with various solute contents, is presented in figure 5(a). From these data, the concentration in the top part of the diffusion cell is then obtained as a function of time. After an initial delay t_0, during which diffusion of the ions becomes established across the thickness of the sample, there is a linear increase with time in the concentration of the solution in compartment No 2. This experiment is performed for two samples, each of them being oriented in such a way that ions may diffuse either along the direction $\vec{a}$ or along the direction $\vec{c}$ of the material. Diffusion of ions in water is also studied with an identical device, i.e., using the same compartment volumes but without any sample and without stirring in compartment No 2. Therefore, direct comparison between diffusivity throughout the material, on the one hand, and within water, on the other hand, may be achieved, as detailed below.

The diffusion coefficient is defined as the constant D in Fick's first law:

$$J = -D\frac{\mathrm{d}C}{\mathrm{d}x} \tag{8}$$

where J is the flux of diffusing species in moles per time per unit of cross-sectional area, C their concentration and $\mathrm{d}C/\mathrm{d}x$ the applied concentration gradient. Equation (8) may be written as

$$\frac{V}{S}\frac{\mathrm{d}C_2}{\mathrm{d}t} = D\frac{C_1 - C_2}{L} \tag{9}$$

where S and L have the same meaning as before, V is the volume of solution in compartment No 2, C_1 and C_2 are the solution concentrations in compartments No 1 and No 2 of the diffusion cell, respectively. Hence,

$$D = \frac{VL}{S(t - t_0)}\ln\left[1 + \frac{C_2}{C_1 - C_2}\right]. \tag{10}$$

Thus, the linear behaviours observed in figure 5(b) for diffusion times greater than t_0, whose values depend both on the geometry of the experiment and on the material, are accounted for

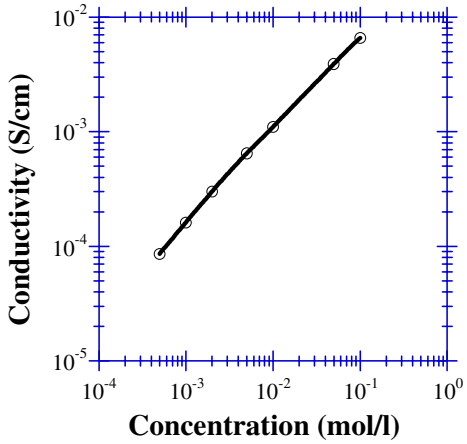

(a)

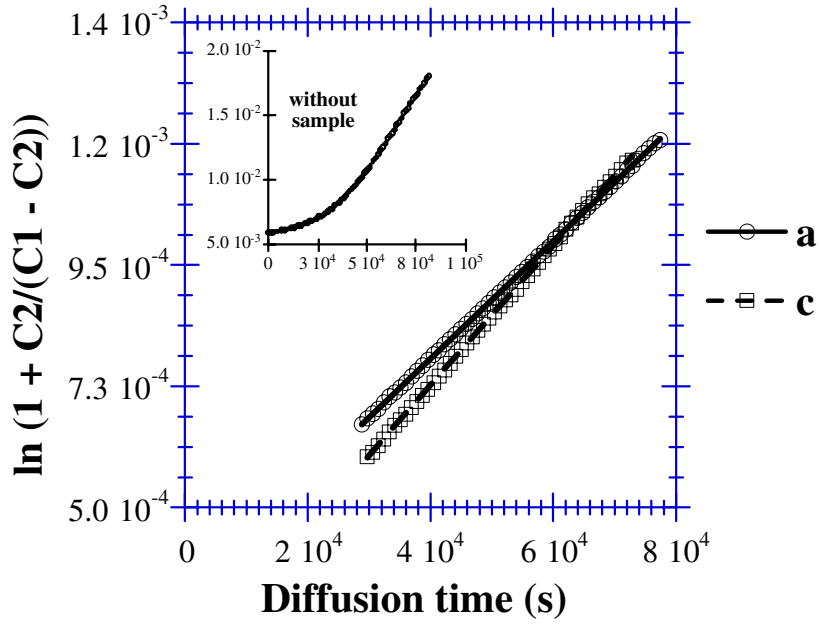

(b)

Figure 5. (a) A calibration curve showing the changes of conductivity of the electrolyte as a function of its concentration. The solid line interpolates between the experimental data. (b) Plots of $\ln[1 + C_2/(C_1 - C_2)]$ versus the diffusion time, where C_1 and C_2 are the concentrations of the ions in the top and in the bottom compartments shown in figure 4, respectively. C_1 and C_2 are calculated from both conductivity measurements and part (a). The experiment is performed for two samples in which diffusion takes place along either direction $\vec{a}$ or direction $\vec{c}$. The inset shows the diffusion of the ions in pure water. Formation factors are calculated from these data and application of equation (10).

by equation (10). The formation factors may then be obtained from the comparison of the slopes of the straight parts of the curves, i.e., corresponding to their steady-state regions; one finds $F_a = D_0/D_a \approx 5.34$ and $F_c = D_0/D_c \approx 6.37$.

3. Theoretical background

The permeability, having the dimension of area, may be seen as representing the cross-section of an effective channel for fluid flow through the pore space. Indeed, according to such a dimensional analysis, k is proportional to a squared length L_0, such that [29]

$$k = \frac{L_0^2}{F}. \tag{11}$$

Such a formula is convenient, since it both expresses the fact that k has the dimension of area and includes the tortuosity and the volume fraction of voids through F. The term L_0 is given different meanings by different authors. Among the various available theories, the three following ones, which are known to yield the best results [5], are examined particularly.

3.1. Kozeny–Carman theory

This is the oldest theory; it deals with porous media comprising capillary pores. It is exact for a bundle of cylindrical tubes having the same length and similar diameters, being non-intersecting and parallel, but possibly tortuous. In such a representation, the so-called 'hydraulic diameter' r_h is defined as being the ratio $2V_p/S_p$, where V_p and S_p are the volume and the surface of the pore space, respectively. Thus, the KC theory states that $L_0^2 = r_h^2/8$ in equation (11) and the permeability reads

$$k = \frac{(V_p/S_p)^2}{2F} = \frac{\Phi(V_p/S_p)^2}{2\tau} \tag{12}$$

where the tortuosity factor τ is the ratio of the capillary length to the sample thickness. Owing to the simplistic hydraulic diameter concept, KC theory is sometimes unable to describe porous systems with wide pore-size distributions. Besides, real pore spaces are multiply connected in a complicated and random way, which is not taken into account by the KC model.

However, for many systems, empirical forms of equation (12) may be derived:

$$k = \frac{\Phi^3}{cS_{sp}^2} \equiv \frac{\Phi^3}{c'\tau S_{sp}^2} \equiv \frac{\Phi^2}{c'F S_{sp}^2} \tag{13}$$

where c is the so-called Kozeny constant ($c = 2$ for cylindrical tubes, while $c \approx 5$ for many materials), c' is an empirical parameter and S_{sp} is the internal accessible surface area per unit volume of solid material. Such formulae are very attractive since they contain one single constant (c or c') which depends weakly on the structure, and other quantities like F, Φ or S_{sp} which both possess a physical meaning and are measurable independently of the permeability [30]. Moreover, these formulae are often good approximations for a lot of very different materials.

3.2. The theory of Johnson, Koplik and Schwartz

In the cases for which the pore system cannot be accounted for using a hydraulic diameter, another definition for the length scale L_0 is required. According to JKS, the new parameter Λ may be derived from measurements of the electrical conductivity of the electrolyte-saturated pore phase. Λ could be written as [31]

$$\Lambda = 2\left(\int |E_0|^2 \,\mathrm{d}V_p\right)\Big/\left(\int |E_0|^2 \,\mathrm{d}S_p\right) = \frac{2}{m_{(\Phi)}S_p/V_p} \neq 2\frac{V_p}{S_p} \tag{14}$$

where E_0 is the magnitude of the local electric field in the pore space and $m_{(\Phi)}$ is a constant close to 1.5. With such a definition, Λ is an intrinsic measure of the dynamically interconnected pore size; it is thus a dynamical length scale directly related to transport, unlike the previous purely geometrical one, $r_h = 2V_p/S_p$ [5, 32].

Then, following Johnson, Koplik and Schwartz, L_0 is such that

$$L_0^2 = c_1 \frac{\Lambda^2}{8} \tag{15}$$

where c_1 is a constant which obeys $1 \lesssim c_1 \lesssim 2$. The exact values depend on the model by which the pore space is described, and are given further on in this paper (section 4).

3.3. The theory of Katz and Thompson

This theory presents another definition of the length scale L_0, which may be written as [33, 34]:

$$L_0^2 = c_2 \delta_c^2. \tag{16}$$

In this equation, c_2 is a constant calculated on the basis of percolation theory and δ_c is a pore-size parameter obtained from mercury porosimetry experiments. Moreover, other works also support the use of intrusion porosimetry for calibrating the pore dimension used in calculating the permeability [6, 39]. δ_c represents the critical pore diameter at which the invading mercury first forms a connected path spanning the sample. It may thus be seen as a percolation threshold in terms of pore diameter and corresponds to a critical pressure of intrusion P_c. It was first suggested [35, 36] and later shown from resistivity measurements [37] that such a critical pressure coincides with the inflection point of the mercury-injection curve and hence to the maximum of its derivative. In other words, δ_c is the abscissa of the maximum of the typical curve of incremental intruded volume versus pore diameter.

The way in which the constant c_2 ($\approx 1/226$) was first calculated by Katz and Thompson was criticized by several authors [5, 29]. The latter proposed other values, always higher than 1/226, and depending on the kind of pores assumed to describe the porous system. As in the case of the parameter c_1 of equation (15), a few formulae are given for c_2 in the next section.

4. The model of pore structure in compressed expanded graphite

4.1. Mercury-intrusion experiment

Porosimetry data were obtained using a Micromeritics PoreSizer 9320 instrument. Mercury is forced to penetrate a sample having a volume close to 0.3 cm^3. For that purpose, the hydrostatic pressure is increased from 0 up to 2070 bar in an equilibration mode which allows mercury to flow into the pores for a specified length of time. The output data give the intruded volume as a function of applied pressure.

The raw injection curve is given in figure 6(a). As discussed below, and similarly to what is supposed for most porous materials, cylindrical pores are assumed. Such an assumption allows one to apply the well-known Washburn equation [38], which assigns a particular pore diameter δ to a given injection pressure P:

$$P = -\frac{4\gamma \cos\theta}{\delta}. \tag{17}$$

$\theta = 130^\circ$ is the contact angle between mercury and graphite, and $\gamma = 485$ dyn cm^{-1} is the surface tension of mercury.

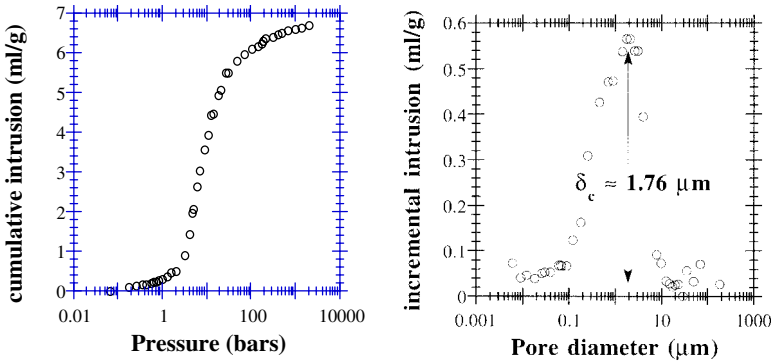

Figure 6. (a) Mercury-injection capillary pressure curve for the sample of compressed expanded graphite. (b) Incremental volume of mercury intruded inside the material as a function of the pore diameter calculated according to Washburn's equation (17). δ_c is the characteristic pore diameter at the continuity threshold in mercury injection.

While flattened pores are intuitively much more likely within compressed expanded graphite and were suspected from the anisotropy of other physical properties [26], cylindrical shapes of pores are conceivable for the following reasons. First, the permeability is governed by narrow throats connecting wider pores within the material, and such necks may be seen as locally cylindrical. Next, even if these wider pores are indeed flattened, effective diameters could be associated with non-cylindrical geometries. In the models described below, the sizes of the pores have wide continuous distributions, and hence non-cylindrical voids could be defined by such effective diameters. Finally, it is well known that mercury porosimetry deals with entry diameters rather than actual pore diameters, just like permeability [39]. Hence it may be assumed that locally cylindrical voids are relevant, since excellent correlations are found between measured permeability and entry pore diameters derived from porosimetry [39]. Besides, simulations have clearly shown that taking into account such capillary resistances at pore entrances leads to greater threshold pressures [40]; thus, the value of δ_c obtained below is assumed to correspond to the unique transport length scale which dominates the magnitude of the permeability.

The curve of incremental intrusion versus pore diameter, the latter being calculated from equation (17), is shown in figure 6(b). According to the previous discussion concerning the percolation of mercury throughout the sample, the critical pore diameter is found to be $\delta_c \approx 1.76$ μm at $P_c \approx 7$ bar. It should be noticed that at the highest pressure of mercury (about 2000 bar), the final density of the sample is not that of pure graphite ($\approx$2200 kg m^{-3}). Surprisingly, it amounts only about 1540 kg m^{-3}, thus corresponding to a residual porosity close to 30%. This result was checked by subjecting another sample of compressed expanded graphite having the same initial density to identical experimental conditions. At this time, no convincing explanation has been found to account for such a high amount of closed porosity still existing at such high pressures. Nevertheless, this means that the relevant porosity is $\Phi = 1 - 140/1540 = 90.91\%$ and not $1 - 140/2200 = 93.64\%$ as supposed *a priori*. Hence, the numerical applications of equations (12) and (14) given in the following section should use the relevant pore volume of the material, that is 0.9091 $\times$ sample volume. Coming back to the quantitative application of Katz and Thompson theory (equation (16)), the constant c_2 whose value depends on the kind of pores considered is required. Thus, the model of the pore space should be now introduced.

4.2. Models considered

For any of the four models considered below, the following assumptions are made. First, the pores have a cylindrical geometry with a diameter δ and a length l. Next, the distribution of their sizes is broad on a logarithmic scale (e.g. log-normal); in other words, the pore sizes vary over several orders of magnitude, exactly as observed in figure 6(b). Indeed, models which take into account only a single pore type [5, 41] are inappropriate for our material.

- Model I. The pores have a constant length $l = l_0$, and only the diameters δ are widely distributed. The parameter Λ and the permeabilities from JKS, on the one hand, and from KT, on the other hand, may be calculated from the following sets of equations, respectively. From [42]:

$$\Lambda_{\mathrm{I}} = \frac{\delta_c}{t+2} \tag{18a}$$

$$k = c_1^{\mathrm{I}} \frac{\Lambda^2}{8F} \qquad \text{with } c_1^{\mathrm{I}} = 16\frac{(2+t)^{4+t}}{(4+t)^{4+t}} \approx 1.39 \tag{18b}$$

$$k = c_2^{\mathrm{I}} \frac{\delta_c^2}{F} \qquad \text{with } c_2^{\mathrm{I}} = 2\frac{(2+t)^{2+t}}{(4+t)^{4+t}} \approx 1.14 \times 10^{-2} \tag{18c}$$

  or from [29]:

$$\Lambda_{\mathrm{I}}' = \frac{\delta_c}{\nu+2} \tag{18d}$$

$$k = c_1^{\mathrm{I}'} \frac{\Lambda^2}{8F} \qquad \text{with } c_1^{\mathrm{I}'} = \frac{1}{4}(2+\nu)^2\left(\frac{1}{2}\right)^{\nu} \approx 1.12 \tag{18e}$$

$$k = c_2^{\mathrm{I}'} \frac{\delta_c^2}{F} \qquad \text{with } c_2^{\mathrm{I}'} = \frac{1}{32}\left(\frac{1}{2}\right)^{\nu} \approx 1.69 \times 10^{-2}. \tag{18f}$$

  In these equations, the parameters t and ν are the critical exponents for the electrical conductivity and the correlation length, respectively. In three-dimensional systems, they are such that $t \approx 1.9$ and $\nu \approx 0.88$ [43, 44].
- Model II. The length is proportional to the diameter with a proportionality constant α: $l = \alpha\delta$ [29]:

$$\Lambda_{\mathrm{II}} = \frac{\delta_c}{2(1+\nu)} \tag{19a}$$

$$k = c_1^{\mathrm{II}} \frac{\Lambda^2}{8F} \qquad \text{with } c_1^{\mathrm{II}} = (1+\nu)^2\left(\frac{1}{3}\right)^{\nu} \approx 1.34 \tag{19b}$$

$$k = c_2^{\mathrm{II}} \frac{\delta_c^2}{F} \qquad \text{with } c_2^{\mathrm{II}} = \frac{1}{32}\left(\frac{1}{3}\right)^{\nu} \approx 1.18 \times 10^{-2}. \tag{19c}$$

- Model III. The pores obey $l = \delta$. It is not clear what makes models II and III different, but their respective authors derive slightly different results. Thus, [42]:

$$\Lambda_{\mathrm{III}} = \frac{\delta_c}{2(1+t)} \tag{20a}$$

$$k = c_1^{\mathrm{III}} \frac{\Lambda^2}{8F} \qquad \text{with } c_1^{\mathrm{III}} = 27\frac{(1+t)^{3+t}}{(3+t)^{3+t}} \approx 2.07 \tag{20b}$$

$$k = c_2^{\mathrm{III}} \frac{\delta_c^2}{F} \qquad \text{with } c_2^{\mathrm{III}} = \frac{27}{32}\frac{(1+t)^{1+t}}{(3+t)^{3+t}} \approx 7.68 \times 10^{-3}. \tag{20c}$$

- Model IV. The pores are sinuous tubes with a curvature R such that $l = \sqrt{R\delta}$ [29, 45]:

$$\Lambda_{\mathrm{IV}} \approx 0.383\delta_c \tag{21a}$$

$$k = c_1^{\mathrm{IV}} \frac{\Lambda^2}{8F} \qquad \text{with } c_1^{\mathrm{IV}} \approx 0.81 \tag{21b}$$

$$k = c_2^{\mathrm{IV}} \frac{\delta_c^2}{F} \qquad \text{with } c_2^{\mathrm{IV}} = \frac{1}{32}\left(\frac{3}{7}\right)^{\nu} \approx 1.48 \times 10^{-2}. \tag{21c}$$

On the basis of these four models and using the experimental values of the permeability, the formation factors F may be calculated and compared.

5. Comparison of the models of pore structure

5.1. Calculated parameters

The numerous previous formulae are now applied in order to compare their results and hence test the applicability of the models. The following quantities are thus calculated:

- Parameter Λ from equation (14), in which $S_p \approx 30\ \mathrm{m^2\ g^{-1}} \times$ sample weight $\approx 33.6\ \mathrm{m^2}$, $V_p = \Phi \times$ sample volume $\approx 7.27 \times 10^{-6}\ \mathrm{m^3}$ and $m_{(\Phi)} \approx 1.5$.
- Parameters Λ_i (i = I, II, III or IV, depending on the model), from equations (18a), (18d), (19a), (20a) and (21a).
- Formation factors $F_{(\Lambda)}$ from equations (18b), (18e), (19b), (20b) and (21b), using the value of Λ calculated above from equation (14).
- Formation factors $F_{(\Lambda_i)}$ (i = I, II, III or IV) from equations (18b), (18e), (19b), (20b) and (21b), now using the different values of Λ_{I}, Λ_{II}, Λ_{III} and Λ_{IV} calculated above. Formations factors calculable from equations (18c), (18f), (19c), (20c) and (21c) are respectively identical.
- Formation factor $F_{(KC)}$ from equation (12).

5.2. Results

The formation factors F_a and F_c are thus calculated for the two directions of measurement defined in section 2 of this paper. The values of all of these quantities are gathered in table 1. It may be seen that only the model for which the lengths of the pores are equal to their diameters is completely consistent in terms of both the dynamical length Λ and the formation factors. It thus seems that KT and JKS theories only lead to the same results if the correct values of the prefactors given in equations (18) to (21) are first derived. This may be achieved by a straightforward comparison of the corresponding calculated formation factors. Under these conditions, the agreement between all of the calculated values of F is even strikingly good with the Kozeny–Carman theory. Also, the values of F_a which are calculated with this model with $l = \alpha$ are close to what was found from the diffusion experiments (see section 2.3). Hence, from the point of view of the permeability, compressed expanded graphite could be seen as a porous medium in which the pores have a wide distribution of sizes but maintain lengths and diameters that are close to each other. Another—and more probable—possibility is that such a description of the material only corresponds to the narrow parts of the pore network, which in fact control the permeability. The diameters of these pore necks would be given by mercury porosimetry (pore entry) and would connect greater flattened voids.

Table 1. Dynamical lengths (Λ, Λ_i) and formation factors (F_a and F_c, depending on the direction of measurement) calculated in the frameworks of the four pore models considered: Λ is calculated from both the pore surface area and the pore volume of the sample (equation (14)); the Λ_i are derived from the critical pore diameter δ_c, and depend on the model: I, II, III or IV (equations (18*a*), (18*d*), (19*a*), (20*a*) and (21*a*)); the $F_{(\Lambda)}$ are obtained from equations (18*b*), (18*e*), (19*b*), (20*b*) and (21*b*) for the given value of Λ, while the $F_{(\Lambda_i)}$ are calculated from the same equations but using the (different) values of Λ_i. Finally, the $F_{(KC)}$ are the formation factors derived from the KC theory (equation (12)).

	Model I: $l = l_0$	Model II: $l = \alpha\delta$	Model III: $l = \delta$	Model IV: $l = \sqrt{R\delta}$
Λ	0.289 μm	0.289 μm	0.289 μm	0.289 μm
Λ_i	0.452 μm or 0.612 μm	0.468 μm	0.304 μm	0.675 μm
$F_{(\Lambda)}$	$F_a = 3.48$; $F_c = 6.43$	$F_a = 3.36$; $F_c = 6.22$	$F_a = 5.18$; $F_c = 9.58$	$F_a = 2.03$; $F_c = 3.76$
$F_{(\Lambda_i)}$	$F_a = 8.52$; $F_c = 15.75$ or $F_a = 12.59$; $F_c = 23.27$	$F_a = 8.82$; $F_c = 16.31$	$F_a = 5.74$; $F_c = 10.01$	$F_a = 11.09$; $F_c = 20.50$
$F_{(KC)}$	$F_a = 5.12$; $F_c = 9.47$	$F_a = 5.12$; $F_c = 9.47$	$F_a = 5.12$; $F_c = 9.47$	$F_a = 5.12$; $F_c = 9.47$

Finally, the following remark should be made. As expected, the hydraulic diameter r_h is not equal to the dynamical one Λ, since

$$r_h = 2 \times \frac{\text{total connected pore volume}}{S_p} \approx 0.433\ \mu\text{m}$$

and

$$\Lambda = 2 \times \frac{\text{effective connected pore volume}}{S_p} \approx 0.30\ \mu\text{m}.$$

Hence, the effective pore volume for fluid transport, which is $(\Lambda/r_h)V_p$, is found to be about 70% of the total pore volume. This result is not surprising, since dead-ends are expected in any random percolating structure. Moreover, such a great percentage of blind pores is responsible for the rather low values of the permeability in compressed EG, considering its high total porosity. In fact, most common materials which possess similar permeabilities have much lower porosities (examples are given in [1]). Besides, it is well known that EG compacted to a density of about 1100 kg m^{-3}, thus having a total porosity of 50%, is completely impermeable and is commonly used as seals and gaskets [10, 14, 46]. Consequently, the volume fraction participating in fluid flow in our highly porous material is much less than the total space available. As shown in the next section, the volume percentages of pores yielding the major contributions to the permeability and to the ionic conductivity are even lower.

6. Calculation of the permeability and formation factor

6.1. Assumptions and discussion

Phenomenological expressions for the permeability and the electrical conductivity that can be determined strictly from mercury-injection data were postulated by Katz and Thompson [34]. It is known that the electrical conductance of a pipe of diameter δ only varies with δ,

whereas its hydraulic conductance varies like δ^3. Thus, according to KT, the electrical (g_e) and hydraulic (g_h) conductances of a porous material may be written as

$$g_e(\delta) = \sigma_0\left(\frac{L}{\delta_c}\right)\delta N(\delta)\Phi \tag{22a}$$

$$g_h(\delta) = A\left(\frac{L}{\delta_c}\right)\delta^3 N(\delta)\Phi \tag{22b}$$

where $N(\delta)$ represents the fraction of connected pore space composed of pore widths of size δ and larger, σ_0 is the conductivity of the electrolyte saturating the pore space and A is a constant factor whose value is such that equations (20*c*) and (22*b*) are compatible with each other. Formulae (22*a*) and (22*b*) are the products of a weight factor (δ or δ^3), which expresses the importance of pore widths of size δ, and a density-of-states term $N(\delta)$, which measures the number of paths composed of pore widths not smaller than δ. As δ changes, the magnitudes of the two factors move in opposite directions, and hence the conductances g_e and g_h assume a maximum value for some particular δ^e_{max} and δ^h_{max}, respectively.

The other assumption of KT is that the pore widths of size δ^e_{max} or δ^h_{max} and larger are the dominant paths for the electrical or the hydraulic problem, respectively. Thus, all connected paths through the pore space composed of lengths $\delta \geqslant \delta^e_{max}$ or δ^h_{max} contribute significantly to the conductance, whereas all others do not and are hence ignored. Then, the electrical conductivity and the permeability are thought to be given by [34]

$$\sigma = \frac{g_e(\delta^e_{max})}{L} = \sigma_0\left(\frac{\delta^e_{max}}{\delta_c}\right)N(\delta^e_{max})\Phi \tag{23a}$$

$$k = \frac{g_h(\delta^h_{max})}{L} = A\left(\frac{(\delta^h_{max})^3}{\delta_c}\right)N(\delta^h_{max})\Phi. \tag{23b}$$

Finally, the definition of the parameters δ^e and δ^h such that

$$\Delta\delta^e = \delta_c - \delta^e_{max} \tag{24a}$$

$$\Delta\delta^h = \delta_c - \delta^h_{max} \tag{24b}$$

and expansions of both $N(\delta^e_{max})$ and $N(\delta^h_{max})$ about δ_c to first order in $\Delta\delta^e$ and $\Delta\delta^h$, respectively, allow one to express the permeability in terms of the conductivity:

$$k = A\left(\frac{(\delta^h_{max})^3}{\delta^e_{max}}\right)\left(\frac{\Delta\delta^h}{\Delta\delta^e}\right)\left(\frac{\sigma}{\sigma_0}\right). \tag{25}$$

Comparison of equations (25), (11) and (16) then leads to

$$A = c_2\delta_c^2\left(\frac{\delta^e_{max}}{(\delta^h_{max})^3}\right)\left(\frac{\Delta\delta^e}{\Delta\delta^h}\right). \tag{26}$$

6.2. Application to compressed expanded graphite

The formation factor and the permeability may be calculated from equations (23*a*), (23*b*) and (26) if the quantities δ^e_{max}, δ^h_{max}, $N(\delta^e_{max})$ and $N(\delta^h_{max})$ are now extracted from the data derived from the mercury-injection experiment. Since the so-called [34, 47] saturation function $N(\delta)$ is the percentage of connected pore space composed of pores with widths of size δ and larger, the mercury volume intruded at pressures lower than P_c should not be taken into account for determining the previous quantities. According to Katz and Thompson, such a small amount of mercury which intrudes the sample prior to reaching the threshold pressure is indeed in defects along the surface and in pores not connected to the first connected cluster. Hence,

the prethreshold volume is subtracted from the volume at $P = P_c$, and the ordinate of the raw injection curve is set to zero at $P = P_c$. The quantity V'_p, defined as the cumulative intrusion minus the prethreshold volume, is plotted as a function of the injection pressure in figure 7(a).

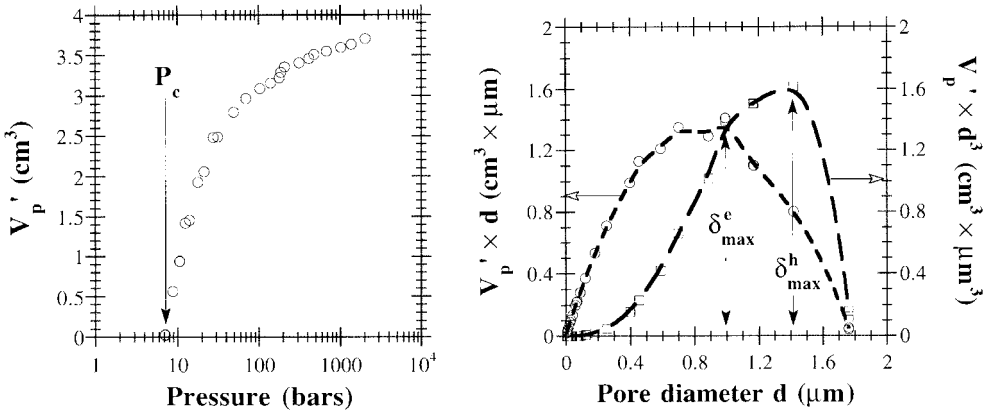

Figure 7. (a) Cumulative intrusion of figure 6(a) minus intruded volume before reaching the threshold pressure P_c (at which the critical pore diameter δ_c is reached), V'_p, plotted as a function of the injection pressure. (b) Relative variations of the electrical and hydraulic conductances, obtained by multiplying V'_p by the factors δ and δ^3, respectively, where δ is the pore diameter. δ^e_{max} and δ^h_{max} are the characteristic pore diameters for electrical and hydraulic conductions, respectively.

The relative variations of the electrical and hydraulic conductances $g_e(\delta)$ and $g_h(\delta)$ are obtained by multiplying V'_p by the factors δ and δ^3, respectively. The resulting curves are displayed in figure 7(b). Their maxima correspond to the optimum paths for the conductivity (δ^e_{max}) and for the permeability (δ^h_{max}). The characteristic pore diameters for electrical and hydraulic conduction are thus found to be $\delta^e_{max} \approx 0.99$ μm and $\delta^h_{max} \approx 1.42$ μm, respectively. The saturation functions on the most effective paths may also be derived from figure 7(b); they are such that $N(\delta_c) = 0$, $N(\delta^e_{max}) = V'_{p(\delta^e_{max})}/V'_{p(max)} \approx 38.3\%$ and $N(\delta^h_{max}) = V'_{p(\delta^h_{max})}/V'_{p(max)} \approx 15.3\%$, where $V'_{p(max)}$ is the maximum value of V'_p, i.e., that at the greatest injection pressure. Consequently, as suggested before, these fractions of connected voids composed of pores of sizes greater than δ^e_{max} or δ^h_{max} are relatively low. These values of $N(\delta^e_{max})$ and $N(\delta^h_{max})$ are in fair agreement with what has been found for various rocks having permeabilities close to those of our material [34, 47]. Finally, such data mean that the effective percentage of total pore space is even lower, being only about 21% for the conductivity and about 8% for the permeability.

The formation factor and the permeability can be now calculated. According to equation (23*a*), F is such that $F \approx 5.10\ F_a$. The constant prefactor A of equation (25), which is required in the calculation of the permeability, is obtained by putting the numerical values of each term in (26), and thus $A \approx 1.857 \times 10^{-2}$ 1/54. This result is somewhat different from that of KT, who obtained $A \approx 1/89$. The permeability is now calculated with equation (23*b*): $k \approx 4.17 \times 10^{-15}$ m^2 k_a. It may be seen that these results are extremely close to the experimental values given in section 2. In our opinion, the fact that F_a and k_a rather than F_c and k_c are recovered originates from the penetration of mercury inside the sample being easier along direction $\vec{a}$ than along the c-axis. Thus, the critical pore size δ_c is reached with mercury

invading the material more rapidly via the voids between the edges of the graphite particles (the xy-plane in figure 1) than via those between the surfaces of carbon sheets. Consequently, the optimum paths for both the conductivity and the permeability are essentially those of the direction $\vec{a}$.

7. Conclusions

The permeation of a gas as well as the diffusion of ions throughout the pore space of a cube made of compressed expanded graphite have been investigated. The corresponding measurements made along two orthogonal directions lead to anisotropic experimental values of both the permeability k and the formation factor F. Mercury porosimetry was also performed on the material. Several parameters such as characteristic pore diameter δ_c and saturation functions were derived from the mercury intrusion data. Substitution of δ_c in various equations has shown that different theories give similar results as long as a single model is considered, that for which the pores may be seen as capillary tubes having both a wide distribution of sizes and a length close to the diameter (the $l = \delta$ model). This finding is somewhat striking for a material in which flattened pores are expected, but probably reflects the fact that narrow and roughly cylindrical throats dominate both the mercury intrusion and the transport properties.

Next, the equation of Katz and Thompson linking k and δ_c was applied with a suitable constant prefactor, i.e., that corresponding to the model with $l = \delta$. However, it should be stressed that the latter was found to be relevant only thanks to similar results being obtained simultaneously in the framework of KT, KC and JKS theories. It thus seems that all of these models need to be compared before being applied; otherwise unsuitable constant prefactors could be used, leading to a poor agreement with the experimental data. The permeability calculated in this way was thus found to agree remarkably well with the measured value. Nevertheless, k being anisotropic, only one of the two components of the permeability tensor was recovered. Similarly, the formation factor calculated according to various theories was found to be very close to the measured value. Again, KT and JKS theories were shown to work correctly, as was the Kozeny–Carman model which was shown to give unexpectedly good results.

We now aim to study the transport properties within the pore space for a series of samples of expanded graphite compressed at various densities. In particular, several relationships linking permeability and porosity will be tested for these materials and should provide more information about the pore structure.

Acknowledgments

The authors gratefully acknowledge the assistance of N Cohaut and J M Guet from CRMD, University of Orléans (France), in performing the mercury porosimetry experiment. The authors are also grateful for the financial support of ECODEV–CNRS through the GDRE 'Adsorbants Carbonés et Environnement' and the Council of the Région Lorraine.

References

[1] Scheidegger A E 1974 *The Physics of Flow Through Porous Media* 3rd edn (Toronto: University of Toronto Press)
[2] Dullien F A L 1979 *Porous Media—Fluid Transport and Pore Structure* (New York: Academic)
[3] Sahimi M 1995 *Flow and Transport in Porous Media and Fractured Rocks* (Weinheim: VCH)
[4] Torquato S 1994 *Physica* A **207** 79

[5] Schwartz L M, Martys N, Bentz D P, Garboczi E J and Torquato S 1993 *Phys. Rev.* E **48** 4584
[6] Reed J S 1993 *J. Am. Ceram. Soc.* **76** 547
[7] Walsh J B and Brace W F 1984 *J. Geophys. Res.* **89** 9425
[8] Stevens R E, Ross S and Wesson S P 1973 *Carbon* **11** 525
[9] Klatt M, Furdin G, Hérold A and Dupont-Pavlovsky N 1986 *Carbon* **24** 731
[10] Chung D D L 1987 *J. Mater. Sci.* **22** 4190
[11] Yoshida A, Hishiyama Y and Inagaki M 1991 *Carbon* **29** 1227
[12] Inagaki M and Nakashima M 1994 *Carbon* **32** 1253
[13] Celzard A, Marêché J F, Furdin G and Puricelli S 2000 *J. Phys. D: Appl. Phys.* **33** 3094
[14] Chung D D L 2000 *J. Mater. Eng. Perform.* **9** 161
[15] Toyoda M and Inagaki M 2000 *Carbon* **38** 199
[16] Savoskin M V, Yaroshenko A P, Shologon V I, Kapkan L M, Lyubchik S B and Savsunenko O B 2000 *Proc. Eurocarbon 2000: 1st World Conf. on Carbon (Berlin)* p 673
[17] Shen W, Wen S, Cao N, Zheng L, Zhou W, Liu Y and Gu J 1999 *Carbon* **37** 356
[18] Pajak J, Krzesińska M, Swiderska K, Furdin G, Marêché J F and Puricelli S 2000 *Proc. Eurocarbon 2000: 1st World Conf. on Carbon (Berlin)* p 531
[19] Marêché J F, Bégin D, Furdin G, Puricelli S, Pajak J, Albiniak A, Jasienko-Halat M and Siemieniewska T 2001 *Carbon* **39** 771
[20] Balat M and Spinner B 1993 *Heat Recovery Syst. Chem. Heat Pumps* **13** 277
[21] Pons M, Laurent D and Meunier F 1996 *Appl. Therm. Eng.* **16** 395
[22] Eun T H, Song H K, Han J H, Lee K H and Kim J N 2000 *Int. J. Refrig.* **23** 64
[23] Han J H, Cho K W, Lee K H and Kim H 1998 *Carbon* **36** 1801
[24] Celzard A, Krzesińska M, Bégin D, Marêché J F, Puricelli S and Furdin G 2001 *Carbon* submitted
[25] Puricelli S, Marêché J F, Bégin D and Celzard A 2000 unpublished results
[26] Krzesińska M, Celzard A, Marêché J F and Puricelli S 2001 *J. Mater. Res.* **16** 606
[27] Celzard A, Krzesińska M, Marêché J F and Puricelli S 2001 *Physica* A **294** 283
[28] Lide D R (ed) 1998–1999 *Handbook of Chemistry and Physics* 79th edn, vol 5 (Boca Raton, FL: Chemical Rubber Company Press) p 93
[29] Le Doussal P 1989 *Phys. Rev.* B **39** 4816
[30] Berryman J G and Blair S C 1986 *J. Appl. Phys.* **60** 1930
[31] Johnson D L, Koplik J and Schwartz L M 1986 *Phys. Rev. Lett.* **57** 2564
[32] Kostek S, Schwartz L M and Johnson D L 1992 *Phys. Rev.* B **45** 186
[33] Katz A J and Thompson A H 1986 *Phys. Rev.* B **34** 8179
[34] Katz A J and Thompson A H 1987 *J. Geophys. Res.* **92** 599
[35] de Gennes P G and Guyon E 1978 *J. Méc.* **17** 403
[36] Chatzis I and Dullien F A L 1977 *J. Can. Petrol. Technol.* **16** 97
[37] Thompson A H, Katz A J and Rashke R A 1987 *Phys. Rev. Lett.* **58** 29
[38] Van Brakel J, Modrý S and Svatá M 1981 *Powder Technol.* **29** 1
[39] Lukasiewicz S J and Reed J S 1988 *J. Am. Ceram. Soc.* **71** 1008
[40] Tsakiroglou C D and Payatakes A C 1990 *J. Colloid Interface Sci.* **137** 315
[41] Saeger R B, Scriven L E and Davis H T 1991 *Phys. Rev.* A **44** 5087
[42] Banavar J R and Johnson D L 1987 *Phys. Rev.* B **35** 7283
[43] Fisch R and Brooks Harris A 1978 *Phys. Rev.* B **18** 416
[44] Sahimi M 1994 *Applications of Percolation Theory* (Bristol, PA: Taylor and Francis)
[45] Banavar J R, Cieplak M and Johnson D L 1988 *Phys. Rev.* B **37** 7975
[46] Carbone-Lorraine Group (France) 1990 Papyex®, flexible graphite *Technical Paper*
[47] Thomson A H, Katz A J and Krohn C E 1987 *Adv. Phys.* **36** 625